01 Jun 2023

Preliminary Bond Capacity Exploration between Monolayer Graphene and Cementitious Composites

Yanping Zhu

Chuanrui Guo

Genda Chen
Missouri University of Science and Technology, gchen@mst.edu

Recommended Citation

Y. Zhu et al., "Preliminary Bond Capacity Exploration between Monolayer Graphene and Cementitious Composites," *Results in Engineering*, vol. 18, article no. 101075, Elsevier, Jun 2023.
The definitive version is available at https://doi.org/10.1016/j.rineng.2023.101075

Results in Engineering 18 (2023) 101075

Contents lists available at ScienceDirect

Results in Engineering

journal homepage: www.sciencedirect.com/journal/results-in-engineering

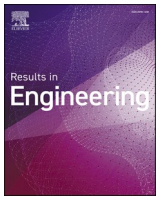

Preliminary bond capacity exploration between monolayer graphene and cementitious composites

Yanping Zhu [a,*], Chuanrui Guo [b,**], Genda Chen [a]

[a] Department of Civil, Architectural, and Environmental Engineering, Missouri University of Science and Technology, Rolla, 65401, Missouri, USA
[b] Institute of Urban Smart Transportation & Safety Maintenance, College of Civil and Transportation Engineering, Shenzhen University, Shenzhen, China

ARTICLE INFO

Keywords:
Monolayer graphene
Cementitious composites
Bond
Pullout test
Chemical vapor deposition

ABSTRACT

This study aims to explore bond capacity between monolayer graphene and cementitious composites for the first time through a pullout test. The low-pressure chemical vapor deposition method was used to synthesize monolayer graphene on the copper substrate to be embedded in the mortar made by the briquette mold. The bond capacity between them was higher than the tensile strength of the copper sheet with as-grown monolayer graphene on the surface since all specimens failed in fracture with embedment length of more than 30 mm. The monolayer graphene enhanced the copper tensile fracture stress and normalized energy during the test as the copper sheet width increased. This short communication explores a new path to quantify the bond between the monolayer graphene and the mortar to promote the understanding of the behavior of graphene-enhanced cementitious composites.

1. Introduction

Graphene is two-dimensional carbon atom single layer with a hexagonal lattice, exhibiting excellent and unique mechanical performance (such as large specific surface area, ultra-low bending rigidity and excellent thermal and electrical properties) [1–3]. Various theoretical studies and practical applications [4,5] have been conducted on graphene-based cementitious composites to enhance inherent brittleness nature at nanoscale [6–10] and resulting mechanical performance because of the improvement on hydration and microstructure (i.e., nano-filler, nucleation template and bridging crack). However, bond capacity between monolayer graphene and cementitious composites has not been directly studied yet, while it can influence reinforcement effectiveness.

In this study, the bond capacity between the monolayer graphene and cementitious composite is explored. The monolayer graphene grows on the copper substrate first using chemical vapor deposition method [11–16] in our lab. One research hypothesis is that an ideal bond (i.e., high bonding strength and adhesion energy of 0.72 J m^{-2}) between graphene and copper [17–19], and the interatomic force between graphene and metal is stronger than the typical van der Waals force between graphene and a dielectric material due to increasing electronic density at the interface. This hypothesizes the bond failure first between graphene and cementitious composites and motivates the pullout test design. The copper sheets with as-grown graphene on the surfaces are embedded into the mortar made by the briquette mold. The pullout test method has been used to investigate the steel fiber-matrix bond performance in fiber reinforced cementitious composites [20–22]. The failure modes, load-extension curves, and normalized energies of all specimens with varying dimensions are presented to identify the lower limit bond capacity between the monolayer graphene and mortar. This study inspires new insights into the test method design for graphene-cementitious composites bond capacity exploration.

2. Experimental program

2.1. Procedures for graphene grown on the copper sheet

Chemical vapor deposited method was used to grow graphene on the copper substrate. Fig. 1(a) and (b) shows this graphene synthesis process in the lab. The mass flow controller regulated the volume of gas that flowed into the chamber (quartz tube) for reaction. A 25 mm × 100 mm copper foil (99.9%, Alfa Aesar 13380) with a thickness of 125 μ m was soaked in acetic acid (99.7%, Sigma Aldrich 695092) for two days and

* Corresponding author.
** Corresponding author.
E-mail addresses: yz6d7@mst.edu (Y. Zhu), cguo@szu.edu.cn (C. Guo).

https://doi.org/10.1016/j.rineng.2023.101075
Received 24 February 2023; Received in revised form 25 March 2023; Accepted 4 April 2023
Available online 5 April 2023

then cleaned with deionized water, isopropyl alcohol, and acetone before the copper foil was placed in the chemical vapor deposition chamber. A 5-sccm (standard cubic centimeter per minute) hydrogen flowed into the chamber for 30 min, and a 5-sccm methane as precursor flowed into the chamber for 10 min at 1030 $^{\circ}C$ under ~100 mTorr vacuum pressure before cooling down to room temperature to synthesize monolayer graphene on the copper foil surface. The copper foil with as-grown graphene was cut into desirable size (i.e., length and width) for use later. As shown in Fig. 1(c), Raman spectrum was used to validate the presence of monolayer graphene. It is found that the intensity ratio (I_G/I_{2D}) of characteristic G and 2D peaks of monolayer graphene at 1600 and 2650 cm^{-1} is 2.11.

2.2. Specimen preparation and pullout test

The briquette mold fabricated specimen (Fig. 2(a)) and the pullout test setup (Fig. 2(b)) were applied in the experiment to analyze possible bond capacity between the monolayer graphene and mortar. The specimen was separated into two equal halves, namely a fixed half and a pullout half. A 3D printed PVC (i.e., polyvinyl chloride) separator was used at the middle. This separator had a cross-section of 25 × 25 mm and a thickness of 1.5 mm, which matched the cross section of the mold at the middle. A slot (0.2 mm width) was created at the center of the separator to insert the copper sheet in. The copper sheet with as-grown monolayer graphene passed through the slot and was attached using liquid glue at the edge. Then, the separator with the installed copper sheet was placed at the center of the mold. Finally, the fresh mortar was cast into the mold. This mortar was composed of cement (mass usage: 662 g/L and density: 3.15 g/cm^3), silica fume (42 g/L and 2.20 g/cm^3), fly ash C (413 g/L and 2.70 g/cm^3), river sand (527 g/L and 2.65 g/cm^3), masonry sand (308 g/L and 2.64 g/cm^3), lightweight sand (120 g/L and 1.81 g/cm^3), high range water reducer (13.30 g/L and 1.05 g/cm^3),

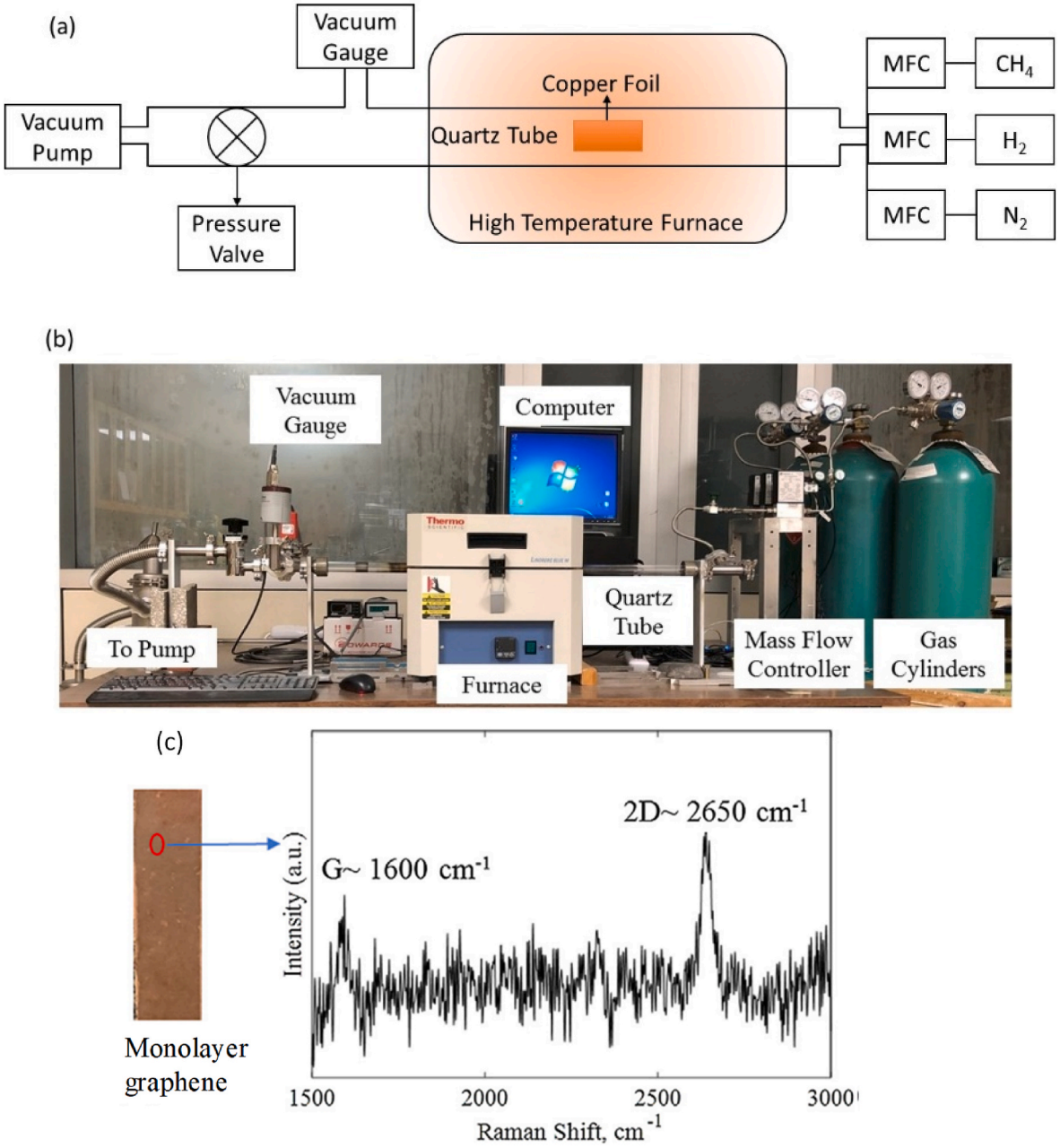

Fig. 1. (a) Schematic illustration (MFC: mass flow controller) (b) low-pressure chemical vapor deposition system (c) monolayer graphene grown on the copper substrate.

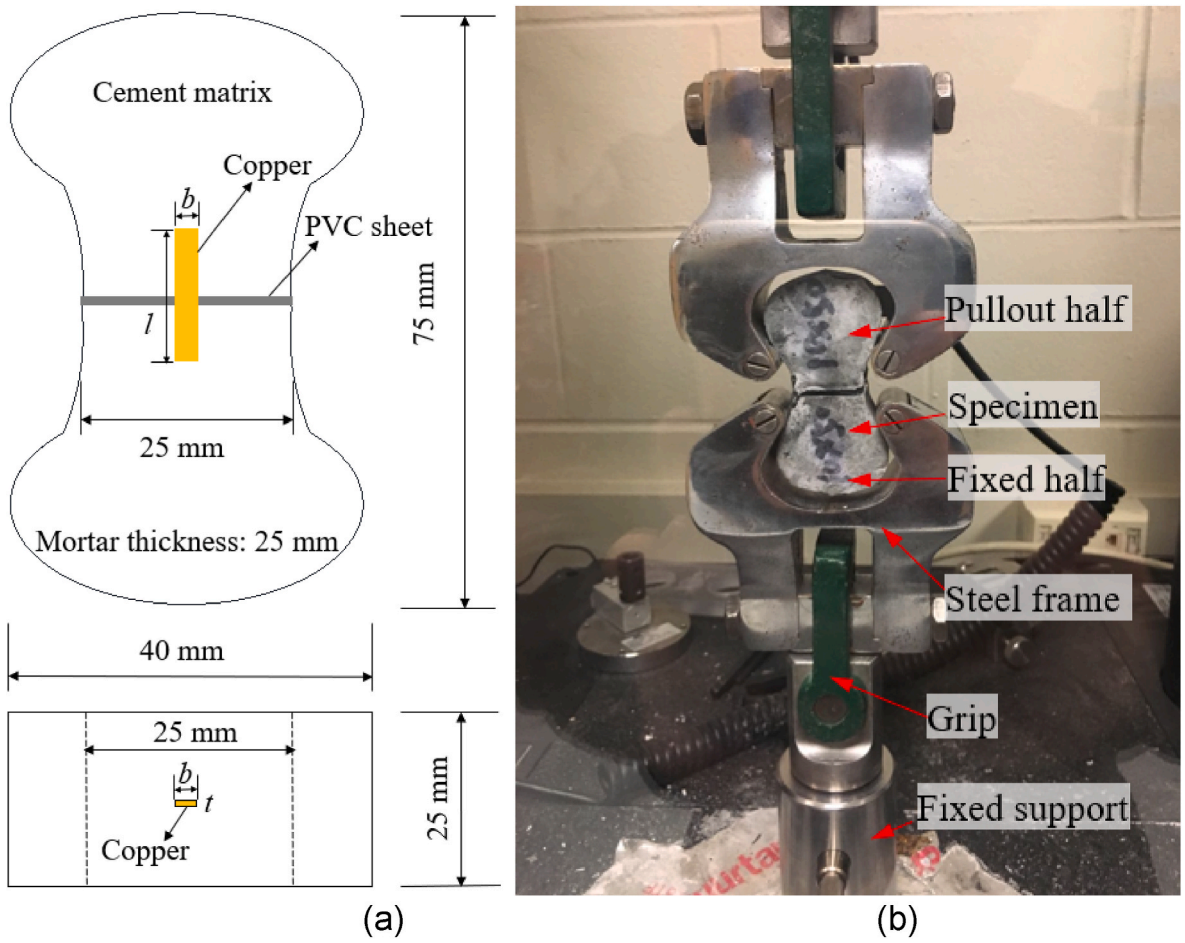

Fig. 2. (a) Geometrical details of mortar and copper sheet (b) pullout test setup.

defoamer (9 g/L and 1 g/cm^3) and water (205 g/L and 1 g/cm^3). Carbon nanotube (3.35 g/L) with 0.30% weight content was added in mortar mixture in an attempt to refine the pore structure of the matrix and fiber-matrix interface (if fiber was included), improve cement hydration, and enable the bridging of cracks at nano or microscale due to the nucleation and filling effect of the nanomaterials.

The specimens were demolded 24 h after casting and cured at normal or steam conditions and then stored in the laboratory environment before testing. Normal curing was in water for 28 days and steam curing at a temperature of about 90 $^{\circ}C$ for three days. Three different copper sheet sample sizes were prepared: 5 mm × 30 mm, 5 mm × 50 mm, and 10 mm × 50 mm (width b x length l), while the thickness (0.127 mm) of all sheets was consistent. Each group had three specimens with the same parameters.

The test setup was shown in Fig. 2(b). An INSTRON testing machine with load capacity of 5 kN was used. The loading rate was 0.5 mm/min to achieve a quasi-static loading. The load versus extension relationship was recorded. We noted that the extension measured from the stroke movement included small elastic deformation of the mortar and the steel frame. Before formal loading, the upper steel grip was raised first to check alignment and make the testing specimen fully contacting with the grip.

3. Results and discussion

All specimens show copper sheet fracture failure at relatively small extensions near the PVC position after the maximum load, and the copper sheet with as-grown graphene on the surface cannot be pulled out from the specimen, which indicates that the failure is controlled by the tensile strength of the copper and monolayer graphene. Fig. 3 shows the load-extension relationships of all specimens, and they show good consistency in each group generally. The experimental phenomenon during the pullout test was described as follows: the pullout started from the interface separation between the mortar and PVC sheet and then, the separation gap gradually expanded due to the extension from the deformation of copper reinforced with monolayer graphene layer. From the test, the copper with monolayer graphene was not actually pulled out from the mortar. We Noted that the interface separation started at a relatively low load since the oil was applied to the surface of the PVC sheet before casting mortar into the briquette mold and the interface between the mortar and PVC sheet was weak.

The maximum tensile stress can be calculated by dividing the maximum load to the cross-sectional area of the copper sheet as shown in equation (1)

$$\sigma_f = \frac{F_{max}}{A_f} \tag{1}$$

where σ_f is the maximum tensile strength (MPa); F_{max} is the maximum load (N); A_f is the cross-sectional area of the copper sheet (mm^2). The energy during the test can be calculated by equation (2) to evaluate the energy dissipation.

$$W_p = \int F(s)ds \tag{2}$$

where W_p is the energy which represents the area under the load-extension curve from mathematic view of point. Due to different widths of the copper sheet, a normalized energy is calculated by dividing

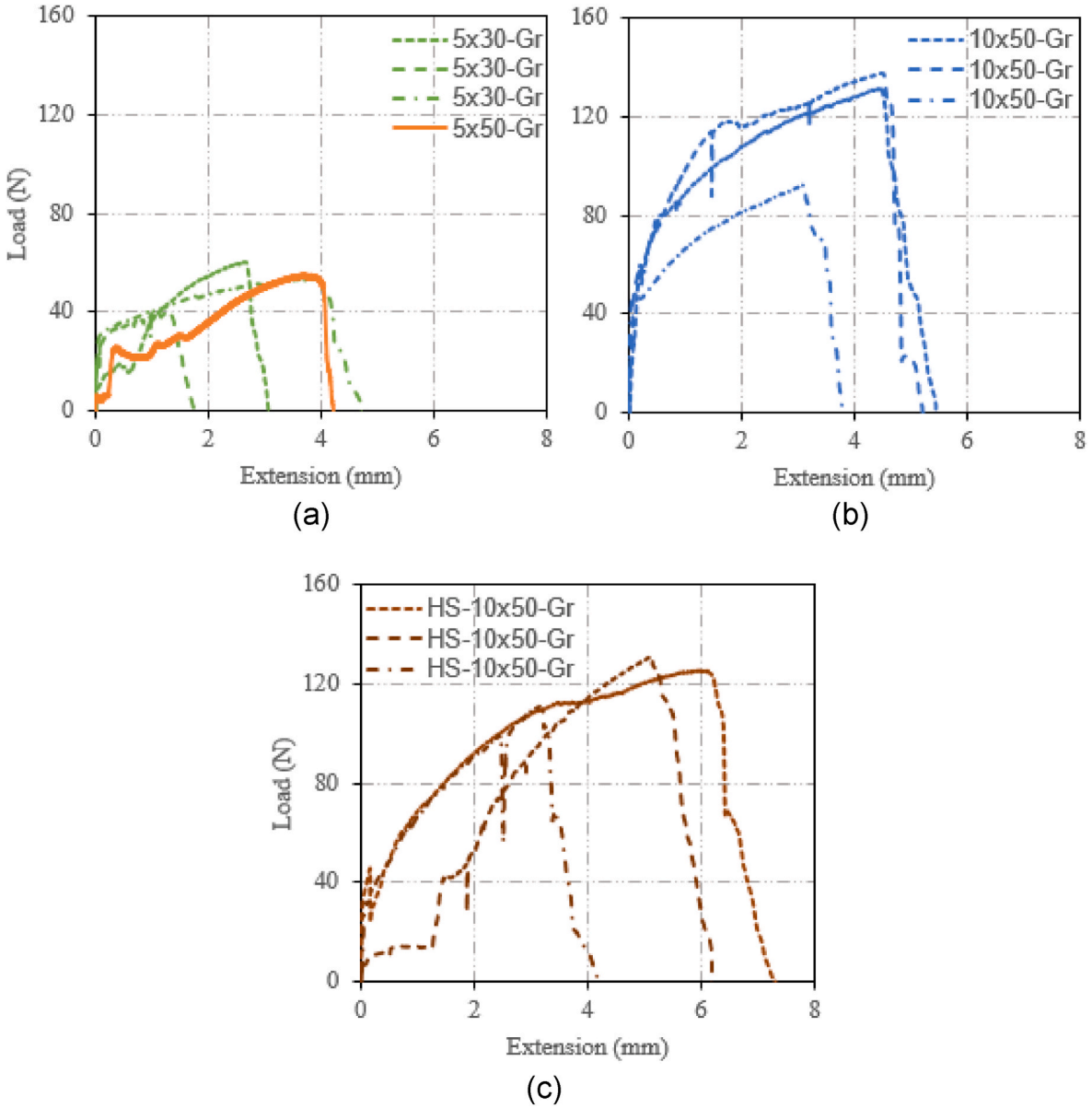

Fig. 3. Load-extension relationships (a) 5 × 30-Gr and 5 × 50-Gr (b) 10 × 50-Gr (c) HS-10 × 50-Gr (Gr: graphene; HS: high temperature steam curing).

equation (2) by the width.

Fig. 4 shows the maximum loads, normal stresses, and normalized energies of different specimens. The error bars are included in Fig. 4(a) and represent the standard deviation of the results of the three samples in the test. As expected, the 5 × 30-Gr and 5 × 50-Gr as well as 10 × 50-Gr and HS-10 × 50-Gr have similar maximum load. However, it is noticed that the normal stress of 10 × 50-Gr/HS-10 × 50-Gr is about 14.5% higher than that of 5 × 30-Gr/5 × 50-Gr. This enhancement is likely attributed to the thin-film graphene on the copper sheet surface and similarly, this reason applies to the enhancement of the normalized energy by 65.5%. From a study by Kim et al. [23], a new material design in the form of Cu-graphene nanolayered composites and Ni-graphene nanolayered composites has been synthesized to achieve ultra-high strengths of 1.5 and 4.0 GPa, respectively from compressing testing of nanopillars. The enhancements of the performance of these metal-graphene nanolayered structures stems from the effective constraint of dislocation propagation across the metal-graphene interface by the monolayer graphene [23]. In addition, the improvement of metal nanolayered composite system strengthened with graphene layer is much better than graphene flakes enhanced metal mixtures due to non-uniform dispersion of graphene flakes within the matrix.

4. Conclusions

In this study, the potential bond capacity between the monolayer graphene and mortar is explored through the pullout test. The bond capacity is higher than the tensile strength of the copper sheet with as-grown monolayer graphene on the surface from the fracture failure of all specimens with minimum embedment length of 30 mm. We also found that the maximum loads are similar for the specimens having the same copper width (regardless of embedment length and curing condition), while as the copper sheet width increases, the enhancements of the tensile fracture stress and normalized energy (by 14.5% and 65.5%, respectively for example) are attributed to the contribution of the monolayer graphene on the substrate surface. Further study directs to analyze full pullout response between monolayer graphene and cementitious composites and the pullout response is to validate molecular dynamics simulation model of the graphene-enhanced cementitious composites to further clarify the role of graphene in the performance improvement. The research achievement can be potentially used for

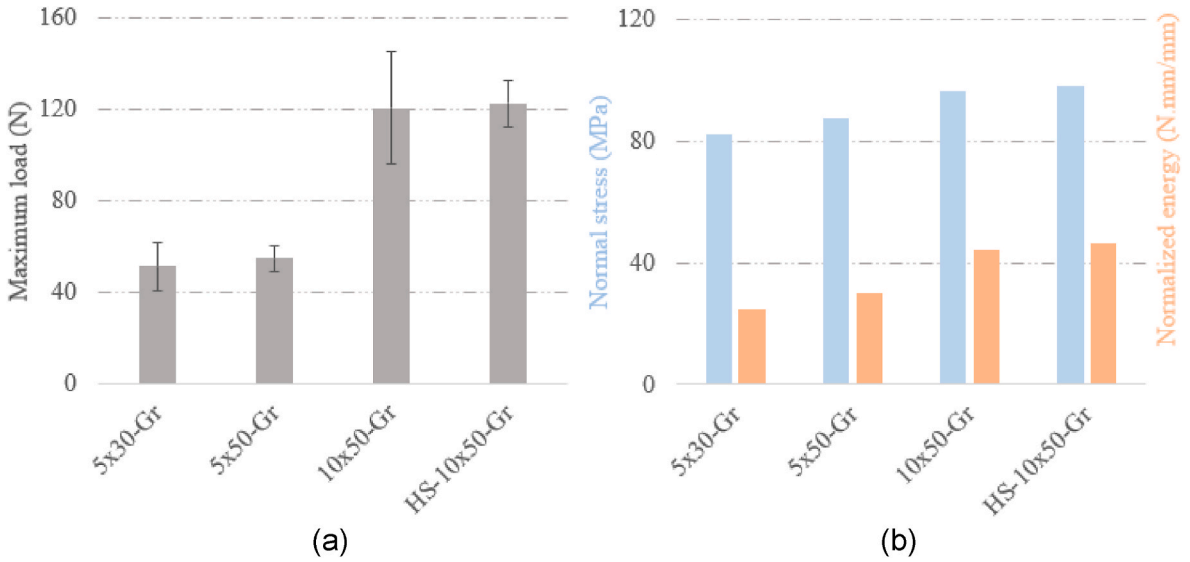

Fig. 4. (a) Maximum load (b) normal tensile stress and normalized energy.

guiding the design of graphene-enhanced cementitious composites.

Credit author statement

Yanping Zhu: Conceptualization, Methodology, Validation, Data curation, Formal analysis, Investigation, Writing original draft, Visualization, Chuanrui Guo: Conceptualization, Methodology, Validation, Reviewing and Editing, Genda Chen: Conceptualization, Methodology, Resources, Reviewing and Editing, Supervision, Project administration, Funding acquisition.

Declaration of competing interest

The authors declare that they have no known competing financial interests or personal relationships that could have appeared to influence the work reported in this paper.

Data availability

Data will be made available on request.

Acknowledgement

Financial support to complete this study was provided by the U.S. Department of Transportation, Office of Assistant Secretary for Research and Technology under the auspices of Mid-America Transportation Center at the University of Nebraska, Lincoln (grant no. 00059709).

References

[1] Y. Wei, R. Yang, Nanomechanics of graphene, Natl. Sci. Rev. 6 (2019) 324–348.
[2] Z. Sun, Z. Yan, J. Yao, E. Beitler, Y. Zhu, J.M. Tour, Growth of graphene from solid carbon sources, Nature 468 (2010) 549–552.
[3] A. Guermoune, T. Chari, F. Popescu, S.S. Sabri, J. Guillemette, H.S. Skulason, T. Szkopek, M. Siaj, Chemical vapor deposition synthesis of graphene on copper with methanol, ethanol, and propanol precursors, Carbon 49 (2011) 4204–4210.
[4] M. Krystek, D. Pakulski, V. Patroniak, M. Górski, L. Szojda, A. Ciesielski, P. Samorì, High-performance graphene-based cementitious composites, Adv. Sci. (2019), 1801195.
[5] H. Yang, H. Cui, W. Tang, Z. Li, N. Han, F. Xing, A critical review on research progress of graphene/cement based composites, Compos. Part A Appl. Sci. Manuf. 102 (2017) 273–296.
[6] A.N. Saleh, A.A. Attar, O.K. Ahmed, S.S. Mustafa, Improving the thermal insulation and mechanical properties of concrete using Nano-SiO2, Res. Eng. 12 (2021), 100303.
[7] C. Cao, Prediction of concrete porosity using machine learning, Res. Eng. 17 (2023), 100794.
[8] S. Sen, H. Li, L. Khazanovich, Effect of climate change and urban heat islands on the deterioration of concrete roads, Res. Eng. 16 (2022), 100736.
[9] M. Hojati, Z. Li, A.M. Memari, K. Park, M. Zahabi, S. Nazarian, J.P. Duarte, A. Radlińska, 3D-printable quaternary cementitious materials towards sustainable development: mixture design and mechanical properties, Res. Eng. 13 (2022), 100341.
[10] R. Nandee, M.A. Chowdhury, A. Shahid, N. Hossain, M. Rana, Band gap formation of 2D materialin graphene: future prospect and challenges, Res. Eng. 15 (2022), 100474.
[11] D.H. Seo, S. Pineda, J. Fang, Y. Gozukara, S. Yick, A. Bendavid, S.K.H. Lam, A. T. Murdock, A.B. Murphy, Z.J. Han, K.K. Ostrikov, Single-step ambient-air synthesis of graphene from renewable precursors as electrochemical genosensor, Nat. Commun. 8 (2017) 1–9.
[12] Y. Li, S. Huang, C. Wei, C. Wu, V.N. Mochalin, Adhesion of two-dimensional titanium carbides (MXenes) and graphene to silicon, Nat. Commun. 10 (2019) 1–8.
[13] Y. Li, C. Wei, C. Wu, Adhesion of silver nano wire graphene composite film, J. Colloid Interface Sci. 535 (2019) 341–352.
[14] C. Guo, L. Fan, C. Wu, G. Chen, W. Li, Ultrasensitive LPFG corrosion sensor with Fe-C coating electroplated on a Gr/AgNW film, Sensor. Actuator. B Chem. 283 (2019) 334–342.
[15] S. Chaitoglou, E. Bertran, Effect of temperature on graphene grown by chemical vapor deposition, J. Mater. Sci. 52 (2017) 8348–8356.
[16] S. Chaitoglou, E. Bertran, Effect of pressure and hydrogen flow in nucleation density and morphology of graphene bidimensional crystals, Mater. Res. Express 3 (2016), 075603.
[17] Z. Xu, M.J. Buehler, Interface structure and mechanics between graphene and metal substrates: a first-principles study, J. Phys. Condens. Matter 22 (2010), 485301.
[18] T. Yoon, W.C. Shin, T.Y. Kim, J.H. Mun, T.S. Kim, B.J. Cho, Direct measurement of adhesion energy of monolayer graphene as-grown on copper and its application to renewable transfer process, Nano Lett. 12 (2012) 1448–1452, https://doi.org/10.1021/nl204123h.
[19] J. Hwang, T. Yoon, S. Jin, J. Lee, T. Kim, S. Hong, S. Jeon, Enhanced mechanical properties of graphene/copper nanocomposites using a molecular-level mixing process, Adv. Mater. 25 (2013) 6724–6729.
[20] Z. Li, Z. Zhang, M. Fei, X. Shi, Upcycling waste mask PP microfibers in portland cement paste: surface treatment by graphene oxide, Mater. Lett. 318 (2022), 132238.
[21] D. Yoo, J. Je, H. Choi, P. Sukontasukkul, Influence of embedment length on the pullout behavior of steel fibers from ultra-high-performance concrete, Mater. Lett. 276 (2018), 128233.
[22] K. Wille, A.E. Naaman, Effect of ultra-high-performance concrete on pullout behavior of high-strength brass-coated straight steel fibers, ACI Mater. J. 110 (2013) 451–461.
[23] Y. Kim, J. Lee, M.S. Yeom, J.W. Shin, H. Kim, Y. Cui, J.W. Kysar, J. Hone, Y. Jung, S. Jeon, S.M. Han, Strengthening effect of single-atomic-layer graphene in metal–graphene nanolayered composites, Nat. Commun. 4 (2013) 2114.